

Dalton Transactions

Accepted Manuscript

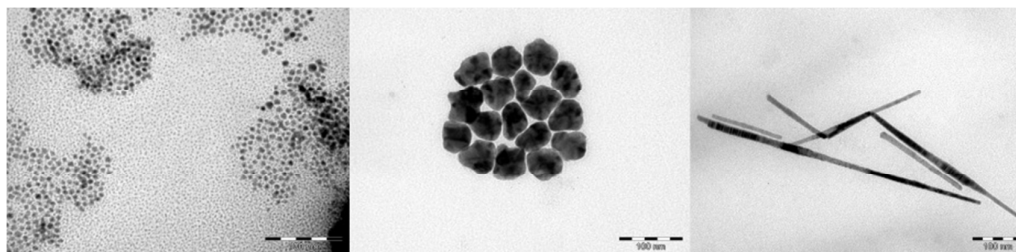


This is an *Accepted Manuscript*, which has been through the Royal Society of Chemistry peer review process and has been accepted for publication.

Accepted Manuscripts are published online shortly after acceptance, before technical editing, formatting and proof reading. Using this free service, authors can make their results available to the community, in citable form, before we publish the edited article. We will replace this *Accepted Manuscript* with the edited and formatted *Advance Article* as soon as it is available.

You can find more information about *Accepted Manuscripts* in the [Information for Authors](#).

Please note that technical editing may introduce minor changes to the text and/or graphics, which may alter content. The journal's standard [Terms & Conditions](#) and the [Ethical guidelines](#) still apply. In no event shall the Royal Society of Chemistry be held responsible for any errors or omissions in this *Accepted Manuscript* or any consequences arising from the use of any information it contains.

Graphical Abstract for the ToC entry

Isotropic and anisotropic NiCo alloy nanoparticles, as well as elongated nanostructures (nanorods, nanowires) with tuned size, shape as well as stoichiometric overall composition are synthesized by employing a H₂-assisted metal-organic chemical approach.

A Study on the Synthesis of Ni₅₀Co₅₀ Alloy Nanostructures with Tuned Morphology through Metal-organic Chemical Routes

Stefanos Mourdikoudis*^a, Vincent Collière, Pierre Fau, Myrtil L. Kahn*

Laboratoire de Chimie de Coordination, CNRS UPR 8241, 205 route de Narbonne, 31077 Toulouse, France

ABSTRACT

NiCo bimetallic nanostructures with various morphologies have been synthesized by using a broad range of solvents, surfactants and precursors that are available in the metal-organic chemical toolbox. Polygonal particles, nanowires and isotropic nanospheres have been obtained, among others. We describe the chemical pathways to achieve anisotropic growth either by an *'in-situ'* seed-mediated approach or by simply selecting suitable reaction media and growth modifiers. We describe the role of a variety of synthetic factors that influence the final material shape of such an alloyed material at the nanoscale. The alloying between cobalt and nickel is evidenced by XRD and HRTEM techniques. Room-temperature ferromagnetic behavior is observed for NiCo nanoparticles and high values for saturation magnetization and coercivity are recorded by SQUID magnetometry. The saturation magnetization value for the NiCo nanostructures is typically set between the corresponding "bulk" ones of cobalt and nickel metals. It always compares to the suggested value of the Ni₅₀Co₅₀ bulk alloy. The synthetic protocols derived from our extensive study are quantitative and versatile, allowing high reaction yields. Although macroscopic characterization techniques evidence the presence of stoichiometric NiCo alloy, we show that in certain cases nanoscale characterization analyses are also needed for a more accurate evaluation of the alloy composition in the atomic level.

1. Introduction

Bimetallic nanostructures are emerging as a new type of fascinating materials¹ because their properties arise typically as a new combination of those of each composing element.² A great improvement is often observed in their physical and chemical properties due to synergistic effects.³ Three main types of organization patterns can be categorized:⁴ a) Core-shell segregated nanoalloys which are composed of a shell of one type of atom (Y) surrounding a core of another (X), though there may be some intermixing between the shells (pattern is usually denoted as core@shell or

*Address correspondence to S. Mourdikoudis, email: mourdik@uvigo.es and M. L. Kahn, email: myrtil.kahn@lcc-toulouse.fr

^a Present address: Departamento de Química Física, Universidade de Vigo, 36310 Vigo, Spain (Tel: 0034986818617)

X@Y), b) subcluster segregated nanoalloys consisting of X and Y subclusters, which may share a mixed interface or may only have a small number of X-Y bonds; heterostructured Pd-Au dimers composed of Pd nanocubes and Au nanoparticles are one example, among others, for this type of organization⁵ and c) mixed X-Y nanoalloys which may possess either an ordered crystalline lattice, or a randomly-mixed pattern, *i.e.* a disordered crystal structure. Ordered and disordered organization types are both common for many bimetallic nano-systems.⁴

The tailored chemical synthesis of metallic alloyed nanostructures is therefore a tricky challenge as compared to single metallic nanocrystals. The control of the composition and the degree of atomic ordering in the alloy is a delicate equilibrium to achieve during the solution-phase reactions. Therefore, it is important to understand, from a fundamental point of view, the mechanisms responsible for the formation of alloyed nanoparticles in the solution phase.⁶ Besides, the synthesis of alloyed nanostructures with anisotropic shapes by liquid-phase processes is an even more challenging goal, because in most cases thermodynamic inclination to minimize the total surface energy is favored and isotropic morphologies are obtained.⁷

As one important class of transition metal alloys, NiCo alloys possess several properties like high mechanical strength, good wear resistance, anticorrosive performance, thermal and electrical conductivity, thermal stability, electrocatalytic activity, and interesting magnetic properties.⁸ Such bimetallic materials could find applications in high-temperature electrochemical devices, as solid oxide fuel cells (SOFCs),⁹ in electromagnetic devices (as magnetic recording devices) as well as in ferrofluid dynamotors and magcards.^{10,11} Moreover, NiCo alloy is known to be highly active for methane drying reforming, and this advantageously promotes the catalyst stability by inhibiting coke formation.¹²

The 'polyol' reduction approach has been widely reported in the literature for the formation of both spherical and anisotropic NiCo alloyed particles. In particular, the Ni- and Co- acetate precursor pair has been frequently used. For example, the preparation of NiCo sub-micron particles targeted for microwave applications¹³ and monodisperse spherical NiCo fine particles¹⁴ were reported. Saravanan *et al.* have reported the polyol reduction of metal acetates to produce PVP-protected NiCo alloy nanoparticles.¹⁵ Ni₂₀Co₈₀ alloy nanoparticles have been prepared by

Luna *et al.*¹⁶ by the polyol reduction of Ni- and Co-acetates in the presence of NaOH. Similarly, dumbbell-like NiCo particles were prepared by the reduction of Co- and Ni- acetates in a sodium hydroxide solution of propanediol.¹⁷ Jayakumar *et al.* have used the combination of PVP and oleic acid during the polyol synthesis of NiCo nanoparticles,¹⁸ while Chakroune *et al.* have reported the formation of nanoplatelets, nanorods and diabolo-like structures by applying a polyol-mediated reduction of metal acetates.¹⁹ Other type of precursors like cobalt and nickel hydroxides have also been employed for the production of quasi spherical NiCo particles.^{20,21} Note that malonate precursors are also reported to avoid the use of any protecting agents for the synthesis of sub-micron NiCo particles.²² Other reported morphologies include nanowires (polyol synthesis),²³ needle-like shape (microemulsion method),²⁴ flower-like morphology (hydrothermal approach),²⁵ handkerchief-like shape (double composite template approach),²⁶ icosahedral shape (solvothermal protocol)²⁷ and even core-shell Ni@Co nanoparticles (microwave-assisted approach).²⁸ Zhou *et al.* have also recently synthesized NiCo alloy hexagonal nanoplates by a solvothermal method. These structures showed high catalytic activity for the hydrolytic dehydrogenation of aqueous ammonia borane under ambient atmosphere at room temperature.²⁹

Monodisperse Ni_xCo_{100-x} alloy nanoparticles with $x = 50$ are only scarcely studied in the literature.⁶ Our group has many years of experience in the organometallic synthesis of monometallic (Co, Ni, Cu, Pt)³⁰⁻³³ and bimetallic nanostructures (NiFe,³⁴ CoAl,³⁵ FeCo³⁶ and FeRh³⁷). We have also successfully synthesized Pt-based bimetallic structures such as CoPt nanoparticles and nanowires³⁸ as well as MnPt nanoparticles.³⁹ Based on the results we recently obtained for the preparation of Ni nanostructures,⁴⁰ we have studied the formation of NiCo stoichiometric nanostructures with controlled morphology. Herein we present the controlled preparation of isotropic NiCo as well as multiangular particles, nanowires and nanorods following a metal-organic approach. The careful choice of the experimental parameters (*i.e.* surfactants, organic solvents, metal precursors and heating conditions) appears to be pivotal for the controlled growth of the bimetallic structures. In this study we highlight that even if macroscopic characterization techniques (e.g. ICP-MS elemental analysis, XRD) show the presence of stoichiometric NiCo alloy, it is necessary to implement characterization techniques at nanoscale level (e.g. STEM/HAADF-EDS) since the relative composition of the two metals in the alloy may

fluctuate at the nanoscale.

2. Experimental

General. All reagents (oleylamine, 80% - 90% C18, 97% primary amines – Acros Organics, hexadecylamine 98% Aldrich, trioctylamine 98% Fluka, ethylenediamine 99% Fluka, oleic acid 99% Aldrich, 1-adamantanecarboxylic acid 99% Aldrich, Ni(COD)₂ 98% Strem, Ni(II) acetylacetonate 98% Strem, Ni(II) acetate tetrahydrate 98% Strem, Nickel stearate (Strem), cobalt stearate (Alfa-Aesar), Co(II) acetate tetrahydrate (Alfa-Aesar), Co(II) acetylacetonate (Fluka), Co(COD)(COT) (Nanomeps), {Co[N(SiMe₃)₂]₂}₂ (Nanomeps) were not further purified but only stored in a glovebox as received to be weighted in completely dry and oxygen-free conditions (O₂ < 1 ppm, H₂O < 1 ppm). Dihydrogen (Air Liquide) might contain only negligible traces of O₂ (<5 ppm) and H₂O (<5 ppm).

Standard airless and water-free techniques (Ar-filled glovebox, vacuum-line, Schlenk tubes and Fischer-Porter bottles) were used, providing either inert or reducing atmosphere during all stages of the synthesis procedure (pre-treatment, reaction, post-preparation handling and product storage). Anhydrous anisole solvent (99.7 %, Sigma-Aldrich) was distilled over Na and degassed before use. Dry pentane and THF were collected from a MB-SPS-800 solvent purification system.

Characterization. Samples for TEM were prepared by evaporation of a drop of each colloidal suspension deposited onto a holey carbon-coated copper grid. The TEM observations were carried out at the “Service Commun de Microscopie Electronique de l’Université Paul Sabatier” (TEMSCAN) in Toulouse on a JEOL JEM 1011 transmission electron microscope operating at 100 kV with a resolution of 4.5 Å. The HRTEM and HAADF/STEM images were recorded using a JEOL JEM 2100F TEM-FEG with an accelerating voltage of 200 kV and a resolution of 2.3 Å. This device is equipped with HAADF detectors and energy-dispersive X-ray spectrometer (EDS). X-ray powder-diffraction (XRD) patterns were measured by a Panalytical MPDPro diffractometer, using Cu-Kα radiation (1.54059 Å). Samples for XRD measurements were sealed in 0.5 mm-diameter Lindemann glass capillaries to prevent any oxidation. Wide-angle X-ray scattering (WAXS) measurements were performed at the CEMES-CNRS in Toulouse. The measurements of the X-ray intensity scattered by the samples irradiated with graphite-monochromatized MoK_α (0.071069 nm) radiation were performed using a dedicated two-axis diffractometer. In the case of WAXS studies, the samples were sealed in 1 mm-diameter capillaries. The magnetic properties were studied using a SQUID magnetometer MPMS5, able to perform measurements in the 2-400 K temperature range and under a magnetic field of 5 T. Elemental analyses were carried out by the ‘Service de microanalyses du Laboratoire de Chimie de Coordination’ (C, H, N) or by Antellis Corporation. (Ni, Co).

Synthesis. Preparation of NiCo nanostructures (refer to Table 1 for a summarized view of all samples):
Sample S1: In a glovebox, 0.5 mmol of Ni(COD)₂ and 0.5 mmol of Co(COD)(COT) were added in a Fischer-Porter bottle containing 10 mmol of HDA in 20 mL of oleylamine. Afterwards the bottle was taken out of the glovebox, the Ar was evacuated and the bottle was pressurized with 3 bars of H₂ for 20 min under stirring. Keeping always the stirring conditions, the bottle was then placed for 24 h in a constant temperature oil bath, previously stabilized at 150 °C. During this time the color of the solution changed from dark purple to black. At the end of the reaction, the dihydrogen was pumped out and the supernatant was removed with a canula. The final product was washed subsequently with pentane and THF. Finally the magnetic powder was dried overnight under dynamic vacuum.

S2: As in S1, but 0.25 mmol of {Co[N(SiMe₃)₂]₂}₂ replaced the 0.5 mmol of Co(COD)(COT).

S3: As in S1, but a surfactant pair was used (ACA/HDA, in 1:2 proportion) instead of an excess of HDA.

- S4: As in S1, but $\{\text{Co}[\text{N}(\text{SiMe}_3)_2]_2\}$ was used instead of $\text{Co}(\text{COD})(\text{COT})$.
- S5: Single use of ethylenediamine (EDA) for the co-reduction of $\text{Co}(\text{COD})(\text{COT})$ and $\text{Ni}(\text{COD})_2$ under 3 bars H_2 , at 120 °C for 48h.
- S6: As in S3, but Co- and Ni- acetates replaced the $\text{Co}(\text{COD})(\text{COT})$ and $\text{Ni}(\text{COD})_2$ respectively.
- S7: Ni-acetate, Co-acetate, anisole, ACA/HDA surfactants (2:1 ratio), 150 °C, 24 h, 3 bars H_2 .
- S8: $\text{Ni}(\text{COD})_2$, $\text{Co}(\text{COD})(\text{COT})$, OAm, 240 °C, 45 min, 3 bars H_2 .
- S9: As in S8, but Co- and Ni- acetates were used as metal sources.
- S10: As in S8, but Co- and Ni- acetylacetonates were used as precursors.
- S11: As in S8, but Co- and Ni- stearates were used as metal sources.
- S12: As in S11, but trioctylamine (TOAm) was used instead of oleylamine (OAm).
- S13: As in S10, but TOAm replaced the OAm.
- S14: As in S10, but 1 eq. of oleic acid was also added.
- S15: As in S11, but 2 eq. of 1-adamantanecarboxylic acid (ACA) were also introduced.
- S16: As in S6, but the heating conditions were modified (240 °C for 45 min and hexadecane instead of anisole).
- S17: As in S11, but hexadecane replaced the OAm and 2 eq. of hexadecylamine (to 1 eq. of total metal concentration) were also added.
- S18: As in S10, but octyl ether was used instead of OAm and 2 eq. of HDA were also inserted.
- S19: Reaction conditions as in sample S11, but $\text{Ni}(\text{acac})_2$ was used instead of Ni-stearate.
- S20: As in S11, but $\text{Ni}(\text{COD})_2$ replaced the Ni-stearate.

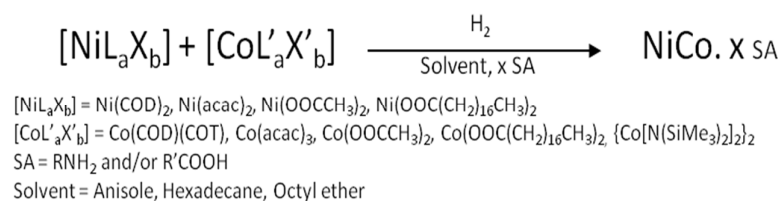
3. Results and Discussion

3.1 Morphological characterization

The survey on existing literature on the controlled alloying of Ni and Co at the nanoscale with tunable Ni/Co composition highlighted that this subject is still a worthy objective from a synthetic point of view.^{14,18,19,23,25,29} Moreover, the Ni/Co precursor ratio may significantly influence not only the composition but also the morphology of the nanomaterials.^{12,41} For these reasons, we focused our study on the chemical synthesis of $\text{Ni}_{50}\text{Co}_{50}$ nanoalloy and explored the possibility to obtain both isotropic and anisotropic morphologies *via* a metal-organic approach. We decided to study the influence of the starting chemical reagents and two different heating conditions: *i*) a low-temperature (low-T) strategy at 150 °C (for 24-48 h) and *ii*) a high-temperature (high-T) strategy, which involves heating at 240 °C (for usually 45 min).

To achieve alloyed nanostructures, we hypothesized that Ni- and Co- precursors having similar thermodynamic and growth kinetic patterns under given reaction conditions were suitable. However, even homologous precursor pairs may not possess identical decomposition behaviors

taking into account that Co^{2+} is, in general, more difficult to reduce than Ni^{2+} . The nucleation rates between these two metals can vary, resulting in a limited control over the final nanoparticle size and composition. Scheme 1 presents the metal-organic approach and the different precursors, stabilizing agents and solvents used during this study. The low-T strategy originates from our previous study on the anisotropic growth control of nanostructured Ni. We demonstrated that low temperature associated with a stable Ni precursor (Ni-stearate) favored the structuring of the reaction media and allowed the anisotropic growth of inherently isotropic crystal structures.⁴⁰ The 'high-T' strategy was chosen because it can promote *i)* a high degree of diffusion between Ni and Co, ensuring an efficient alloy formation at the nanoscale⁴²; *ii)* the decomposition of Co-stearate precursor, which, at 150 °C, is only reduced with a limited yield.



Scheme 1 Synthetic route

3.1.1 The 'low-temperature' strategy

The 'low-T' approach was applied to produce NiCo nanostructures in conditions where kinetic reaction is favored rather than thermodynamic one. Such conditions may influence severely the structure of the final nanomaterial. But such protocol leads to a too slow and only partial decomposition of Co-stearate and $\text{Co}(\text{acac})_2$ compounds. These Co complexes are clearly more stable than the corresponding Ni ones. We therefore focused on the simultaneous use of either a pair of highly reactive precursors [*e.g.* $\text{Co}(\text{COD})(\text{COT})$ or $\{\text{Co}[\text{N}(\text{SiMe}_3)_2]_2\}_2$ and $\text{Ni}(\text{COD})_2$] or the acetate one (*i.e.* Co-acetate and Ni-acetate). The former zerovalent precursors are reactive enough to be decomposed at room temperature in the presence of long alkyl amines and carboxylic acids.⁴³ Among the divalent precursors, those with short molecular chain (especially acetates) can be reduced at moderate temperatures while the reduction of the stearate precursors is the hardest,

needing conditions such as high temperatures and/or longer reaction times.⁴⁴ Such differences will certainly influence the nucleation and growth steps.

Highly reactive precursor pair. The use of an excess of HDA in anisole leads to the formation of large aggregates regardless of the other reaction parameters (samples S1 and S2: see Fig. S-1a and S-1b in ESI respectively). In these conditions, the decomposition of such reactive precursors as well as the nucleation are fast and the amine ligands are not efficient enough to control the reaction kinetics and to prevent the aggregation of the pristine nuclei. The introduction of a bulky carboxylic acid ligand (*i.e.* ACA species) in addition to HDA in a 1:2 ratio, leads to the formation of well-defined nanoparticles of isotropic shapes but with a bimodal size distribution regardless the precursor pair used (NPs with sizes of $\sim 7.1 \pm 1.1$ nm and $\sim 2.5 \pm 0.5$ nm or of $\sim 6.1 \pm 1.4$ nm and $\sim 2.4 \pm 0.7$ nm are obtained for S3 (Fig. 1) and S4 (Fig. S-2) respectively). This suggests that the presence of ammonium-carboxylate species – resulting from the acido-basic reaction between the amine and the carboxylic acid species – prevents the formation of aggregates and allows a good size control of the NPs. However multistep nucleation process is not avoided in these conditions; The employed reaction conditions do not allow an instantaneous decomposition of the whole amount of the precursors. The occurrence of successive nucleation steps, *i.e.* an initial nucleation step leading to the gradual growth of the nuclei to particles - while secondary or ternary nucleation events follow - results in secondary crystals growth stages and at least bimodal size distribution. It has to be noted that additional nucleation steps may take place as a result of the competition between nucleation and growth processes, which is dependent on the reaction parameters. When the synthesis is performed in ethylenediamine (EDA), polydisperse particles with an isotropic shape and a size of 12.2 ± 5.8 nm are obtained together with some agglomerated structures in some areas of the grid (sample S5, Fig. S-3). This result is inconsistent with literature reports which describe the structure-directing coordination template effect of EDA, taking the case of CdS nanowires as an example.⁴⁵ However, this result is in agreement with our previously reported observations on Ni nanostructures prepared in EDA for which isotropic NPs were obtained for different precursor types.⁴⁰ To summarize, upon the use of 'low-T' protocols, the use of sensitive precursor pair does not allow the anisotropic growth of NiCo particles certainly due to a fast nucleation step and the

absence of both efficient growth modifier and structuring of the reaction media.⁴⁰ We have therefore focused our study on precursors which decompose slowly in the employed reaction conditions.

Use of acetate precursors. With Co- and Ni-acetate precursors, the dark purple precursors' solution took a couple of hours to start changing color evidencing a slow decomposition at 150 °C. It should also be noted that the use of dihydrogen as a reductive gas is crucial, as the reduction of both acetate precursors is too slow or practically impossible at 150 °C when using simply inert (*e.g.* Ar atmosphere) conditions. Fig. S-4 presents the obtained NPs in sample S6. Sharp angular structures with a length in the 250-300 nm range and a width of 60-90 nm are observed. Compared to the previously described cases of highly reactive precursor pairs (S3 and S4), the use of acetate precursors (all experimental conditions being equal) allows the preparation of anisotropic structures. The slow decomposition of the above precursors leads advantageously to the continuous release of both metal atoms (Ni and Co) and acetate species until the complete consumption of the precursors. Such a slow decomposition has already been reported to lead to strictly separated nucleation and growth events.⁴⁶ Whether the nuclei grow by the so-called 'oriented attachment' mechanism or by a continuous 'atom by atom' growth after the nucleation step, such conditions appear to favor anisotropic growth. Inversing the ACA/HDA ratio resulted in a quite different shape: nanospatulas with a length around 650-850 nm and a thickness in the 70-160 nm range are formed (Fig. S-5, sample S7). The rather weak contrast and homogeneous hue of the whole object suggests the presence of the aforementioned shape. Such experimental result illustrates how the ACA/HDA ratio can govern the morphology. ACA is a bulky molecule that has already been reported to prevent free surface sites from coordinating with other capping ligands.⁴⁷ Such growth modifier property can lead to nanocrystals with different sizes and shapes depending on its amount and on the other reaction conditions.

In summary, the low-temperature approach enables the preparation of anisotropic structures only when acetate precursors are used. Such anisotropic structures are quite large and their size distributions are relatively wide.

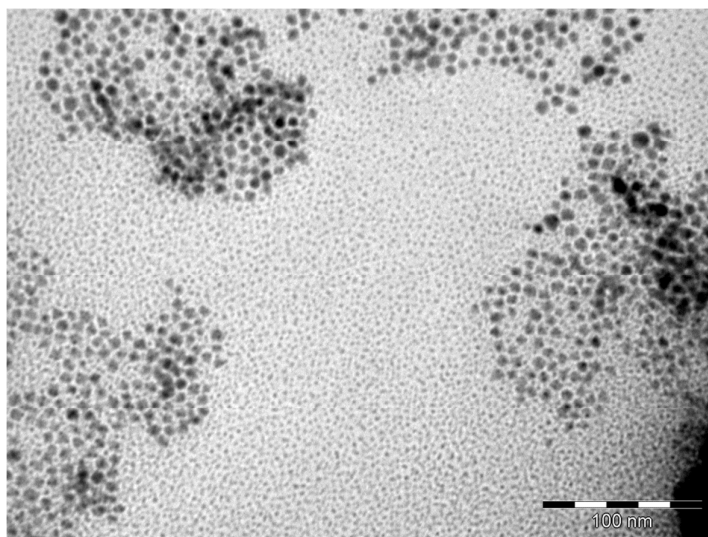


Fig. 1 TEM image for sample S3

3.1.2. *The high-T approach*

The use of OAm as reaction medium. Oleylamine is known to be a good stabilizer for NPs, either with or without the need to use additional co-surfactants.⁴⁸ In a first set of samples, we employed the metal-organic approach using pairs of homologous Ni- and Co- precursors (S8-S11, see table 1). When Ni(COD)₂ and Co(COD)(COT) are used in the absence of a second surfactant (sample S8, Fig. 2a), bimodal isotropic particles with sizes of 7.2 ± 1.3 and 2.4 ± 0.5 nm are obtained, while large polygonal particles are produced when acetate (S9, Fig. 2b), acetylacetonate (S10, Fig. S-6b in Electr. Supp. Info. ESI) and stearate (S11, Fig. S-6a) precursors are used. In these latter cases, the size of the NPs increases when the chain length of the precursor decreases (Table 1). Such tendency may be attributed to the fact that the stearate ligand, being released in the reaction medium during the decomposition of the precursors and possessing a long alkyl chain length, participates to the stabilization of the growing particles contrarily to the acac- and acetate ligands. Because the decomposition is much slower for these precursors than for Ni(COD)₂ and Co(COD)(COT), the nucleation and growth stages will be quite different. Nuclei formation dominates for the latter type of precursors at the expense of particles growth. The observed bimodal population mode might (as for the low-T synthesis) originate from successive nucleation steps. It seems obvious that OAm plays also an important role in particle formation. Indeed, the

use of TOAm leads mainly to large aggregates regardless of the precursors (samples S12 and S13 in Fig. S-7). In addition, some shiny mirror-like color was observed on the reactor walls at the end of the reaction. The bulky TOAm cannot sufficiently participate to the stabilization of the NPs neither to the structuration of the reaction media, thus preventing the formation of well-defined particles.

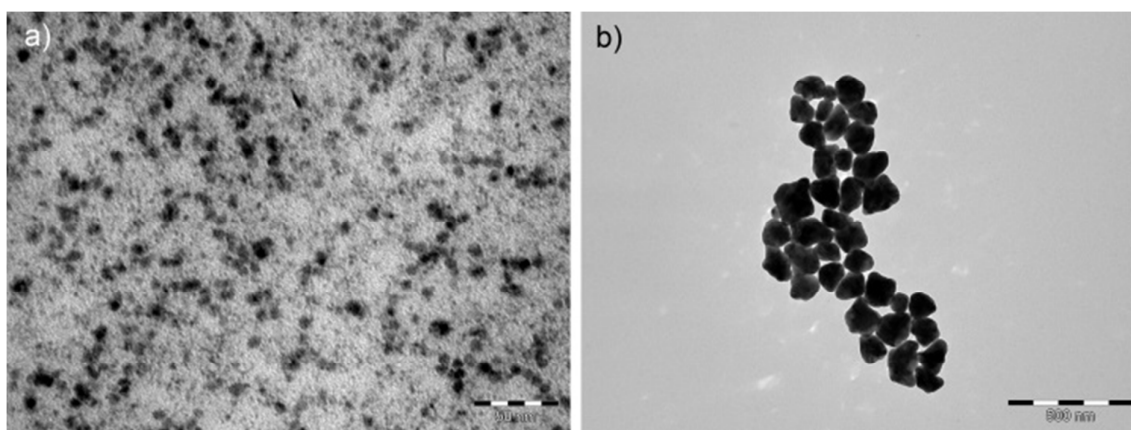


Fig. 2 TEM images for: a) sample S8, b) sample S9. Scale bars are 50 and 500 nm respectively.

Adding co-surfactants. Small isotropic particles (2.4 ± 1.0 nm) were obtained when oleic acid was used as a co-surfactant together with oleylamine (sample S14, Fig. 4b). Such a ligand pair (OAc/OAm) has been extensively employed for the preparation of various nanoparticle systems. Reports on isotropic or nearly spherical morphology are common (see for example Ag,⁴⁹ FePt⁵⁰ and Fe₃O₄ NPs⁵¹). The presence of ammonium-carboxylate ion pairs prevents the growth of relatively large particles in comparison to the sole use of oleylamine. On the other hand, the use of 1-adamantanecarboxylic acid (ACA) did not cause any notable modification compared to the sample prepared in pure OAm (S11) – apart from a size increase to *ca.* 80 nm. A polygonal morphology is similarly obtained (sample S15, Fig. S-8 in ESI). In these experimental conditions (*i.e.* in the presence of OAm only without using any additional solvent), the voluminous ACA molecule leaves a large amount of the particles' surface unprotected, therefore complicating the interaction of the ammonium carboxylate ion pairs with the particles and/or the structuration of the reaction media in comparison to its analogue possessing a linear molecular chain (oleic acid). In particular, contrarily to ACA, oleic acid helps toward a better structuration of the reaction medium. Its long

linear alkyl chains may indeed get together *via* van der Waals interactions or with the corresponding alkyl chains belonging to the amine molecules, also present in the reaction solution.

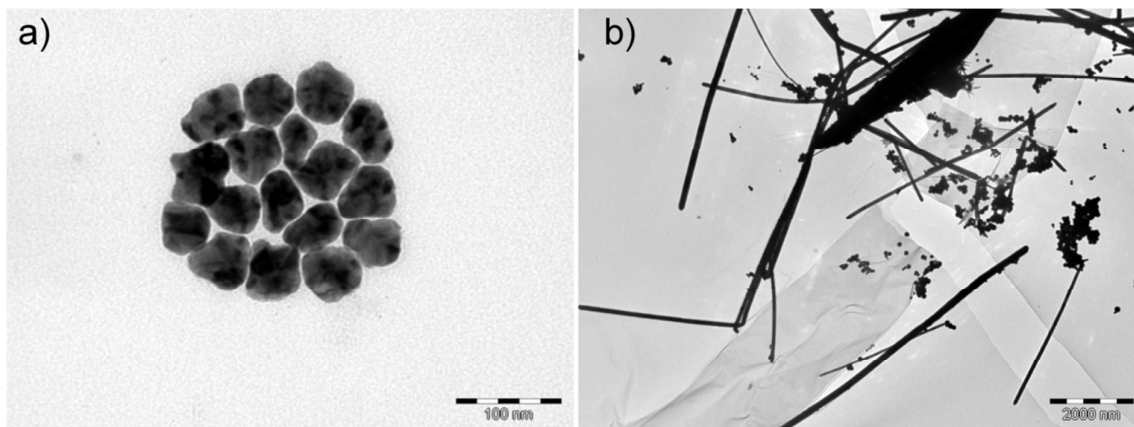


Fig. 3 TEM images for: a) sample S19, b) sample S16. Scale bars are 100 and 2000 nm respectively

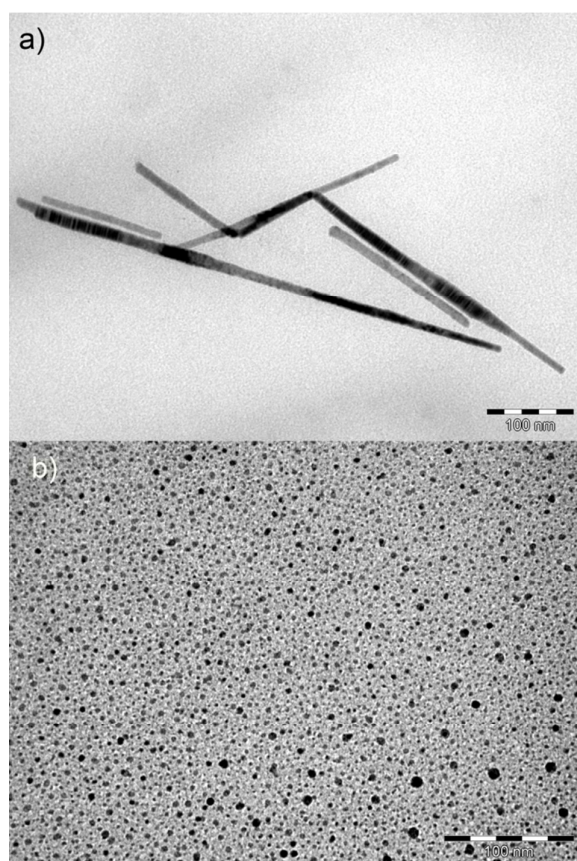


Fig. 4 TEM images for: a) sample S20, b) sample S14. Scale bars: 100 nm

On the role of solvent. The literature survey also evidences that the coordinating or non-coordinating nature of the growth solvent is an important parameter in synthetic chemistry. For a given solvent its proper metal ion coordinating strength can alter reaction kinetics thus affecting the final nanoparticle shape.^{52,53} Solvents such as benzyl ether and phenyl ether contain aromatic rings, which are good electron donors and may interact with the NP's surface. On the contrary, solvents with largely saturated hydrocarbon chains as octyl ether and octadecene are not effective electron donors and they have provided modified nucleation behaviors and altered morphologies in the case of Au/Fe₃O₄ nanoparticles in comparison to the aforementioned coordinating solvents.^{54a} Very recently, Baaziz *et al.* have also reported that the nature of solvent affects the onset of nucleation and growth steps, resulting in different sizes during the synthesis of iron oxide NPs.^{54b} Certainly, such differences in the size and shape of the NPs may also be partly attributed to the varying diffusion behavior of the precursors into the different solvents.

In our study hexadecane showed a preference for nanowire (NWs) formation with a length of several micrometers and a width in the 80-150 nm range (Fig. 3b, sample S16) together with the presence of some aggregated particles. Such a tendency (*i.e.* the formation of long NWs) was also noticed in our recent work upon the single use of Ni-acetate as metallic source in hot hexadecane.⁴⁰ It is possible that the high viscosity of hexadecane (3.34 cP at 20 °C)^{55a} decreases the reduction rate of the precursor and/or participates to the overall structuration of the reaction medium.^{55b} Moreover, the limited electron donating ability of the non-coordinating hexadecane might favor a better control of the growth, preventing further nucleation events once the first nuclei are formed,^{54a} therefore separating the nucleation and growth stages and allowing access to anisotropic nanostructures.^{55b} Nevertheless, the situation is not so simple as the combination of stearate precursors with hexadecane and hexadecylamine (HDA) did not provide elongated structures. Nearly spherical particles of $\sim 65 \pm 11$ nm in size (sample S17, Fig. S-9 in Supp. Information) were obtained in this case. On the other hand, a solvent with different polarity and different coordinating ability than hexadecane, *i.e.* octyl ether, yielded anisotropic nanoparticles with a size of $\sim 76 \pm 13$ nm, while a slight tendency for nanowire growth ($l \sim 2 \mu\text{m}$, $d \sim 30$ nm) was also noticed (Fig. S-10, sample S18, metal acetylacetonates as precursors). Moreover, it has been

reported that NW formation is, in some cases, favored by the use of hexadecylamine ligand.⁵² In our study, HDA was extensively used (samples S1-S4, S6, S7 and S16-S18), but anisotropic shapes were rarely observed. In particular, the use of HDA alone does not readily lead to an anisotropic growth. The only example where a strong tendency for anisotropic growth is observed in the presence of HDA is obtained with sample S16. In this sample, hexadecylamine is combined with ACA ligand in hexadecane and acetate precursors are decomposed at high temperature.

To summarize, the difficulty for a controlled anisotropic growth of NPs is quite usual. To overcome this problem, the growth on previously formed seeds of the same or different composition seems appealing to facilitate the control of the synthesis with regard to the shape tuning as already reported in the case of Au,⁵⁶ CdSe⁵⁷ or hybrid nanoparticles.^{54a}

The use of modified precursor pairs – An *in-situ* seed-mediated approach? In a second set of samples, we changed the precursor pairs by non-homologous precursors all other parameters being equal (samples S19 and S20, to be compared to the series S15-S18). In this case, one of the two precursors will start to decompose earlier than the second one. Thereby, the formed seeds may promote the formation of anisotropic nanoparticles until the complete decomposition of both precursors. The replacement of Ni-stearate by Ni(acac)₂ (sample S19, Fig. 3a) leads to polygonal nanoparticles. Thus, in sample S19, the use of an acetylacetonate precursor instead of the stearate one did not cause any important change in the morphology. On the other hand, the use of Ni(COD)₂ together with Co-stearate (without any further modifications in the reaction parameters) results in highly anisotropic shapes (sample S20, Fig. 4a): Nanowires (*l*~300-600 nm) and nanorods (*l*~150-200 nm) with a width of ~ 10 nm are predominantly observed. The huge difference in the decomposition kinetics between the Ni(COD)₂ and the Co-stearate precursors may provoke the formation of Ni nuclei in an early stage of the reaction. These nuclei could later act as seeds for the one-dimensional growth of the NiCo structure. Stearate ligands, released during the Co-precursor decomposition, certainly help in this anisotropic growth process.⁴⁰ The role of OAm is also critical, as this long-chain amine has been reported to direct the seed-mediated synthesis in a highly anisotropic way.⁵⁸ The discussion of the STEM-EDS results presented in the following section helps

for a better understanding of the phenomena taking place during the growth of sample S20.

3.2 Structural characterization

ICP-MS (Inductively coupled plasma mass spectrometry) elemental analyses. The nickel and cobalt contents in the samples were measured by Antellis Co. Nitric acid was employed for the preparation of samples allowing the determination of the metals' elemental quantities. A large number of samples were analyzed, and all of them presented a Ni/Co ratio between 47/53 to 53/47, *i.e.* very close to the ideally expected equiatomic proportion. These samples included some prepared by the 'high-T protocol' (S11, S14, S16, S18, S19) and others synthesized with the 'low-T protocol' (S3, S4, S6). The total metal content in most of the final nanomaterials was in the 90-95 wt% range. The ferromagnetic property of the nanoparticles which were collected by the stirring magnet at the end of the synthesis and washing procedures facilitated their effective isolation and the removal of the excess surfactants (see also Fig. S-14 and the last page of ESI).

'X-ray' measurements (XRD, WAXS). The XRD patterns of three representative samples (S15, S18, S19) have been indexed by using the JCPDS database (Fig. 5). The peaks at *ca.* 44.4°, 51.7° and 76.2° respectively correspond to the (111), (200) and (220) planes of the *fcc* structure (ICSD coll. Code #108308), characteristic of the equiatomic NiCo alloy. No peaks attributed to oxide or single metal structures are observed. In fact, the above 2 θ angle positions are between the ones of bulk *fcc* Co (44.2 and 51.5°) and those of bulk *fcc* Ni (44.5 and 51.8°) according to the JCPDS files 15-0806 (Co) and 04-0850 (Ni), respectively. Some reports consider that such slight shifts in the XRD peak positions are enough to confirm the alloy formation.^{21,59} However some authors consider that these small differences in the XRD peaks cannot lead to completely safe claims for alloy formation.⁶⁰ For this reason, we decided to carry out nanoscale HRTEM-STEM-EDS analyses in selected samples, as shown below. Our results are in agreement with the crystallization behavior of the alloy in its bulk form, as well as with other research works on stoichiometric NiCo nanoparticles.^{6,61} Indeed, according to the reported phase diagram of NiCo binary bulk alloys, Co and Ni form a continuous series of solid solution alloys which crystallize in the *fcc* phase for compositions above 30 at.% (atomic percentage) of Ni, while alloys with Ni composition in the 20–30 at.% range crystallize in a

mixture of fcc and hcp phases.⁶² The absence of any hcp-phase peaks in the XRD patterns therefore strengthens the elemental analysis results showing the expected equiatomic alloy composition. Such results were confirmed by WAXS experiments exhibiting peaks which also fit well with the Ni₅₀Co₅₀ fcc alloy (Fig. S-11 in ESI, samples S19 and S18).

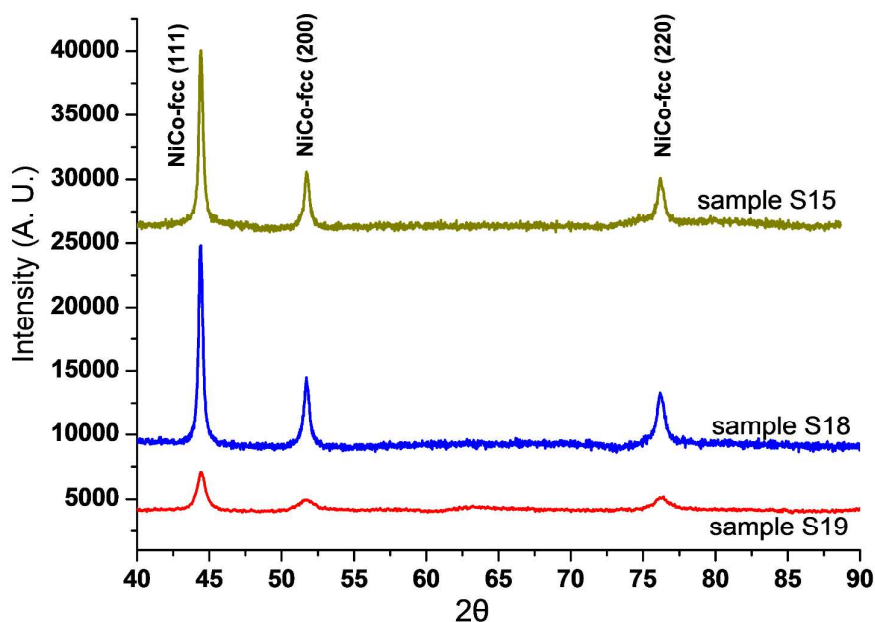


Fig. 5 XRD measurements for samples S15, S18 and S19

HRTEM analyses (STEM/HAADF – EDS). Fig. 6b shows an HAADF-STEM image for sample S10. Elemental mapping by STEM-EDS (Fig. 6c, 6d) illustrates that Ni and Co metals are very well mixed in the particles thus displaying a high degree of alloying. The high temperature reaction protocol possibly promoted the alloying between nickel and cobalt atoms in a common crystal lattice. Moreover, the use of homologous precursors (*i.e.* Ni- and Co- acetylacetonates) can help toward a more ‘homogeneous’ nucleation and growth behavior. The EDS spectrum associated to the HRTEM image of Fig. 6a and 6b provides a Ni/Co ratio equal to 53/47 in this sample, very close to the 50/50 ratio of the starting metallic-source reagents (Fig. S-12 in ESI).

Nevertheless, STEM-EDS analyses performed on heterogeneous samples (*i.e.* sample S20 consisting in a mix of different anisotropic nanostructures like nanowires, nanorods and tripods)

showed that the composition distribution of nickel and cobalt is not that uniform in all the sample volume. For instance, the 'thinner' tripods observed in S20 are Co-rich, while some more elongated and thicker structures appear to be Ni-rich (Fig. S-13 in ESI). Probably, the difference in the decomposition behavior between Ni(COD)₂ and Co-stearate precursors leads to the formation of Ni seeds in an early reaction stage. Such seeds may aid the growth in elongated structures in a first step, but they cannot allow at the same time a homogeneous distribution between both metals in the alloy. The nickel seeds seem to play an important role for such anisotropic morphologies. Indeed, we have observed that the single decomposition of Ni(COD)₂ or Co-stearate in OAm did not favor the one-dimensional growth (not shown here). Such results allow us to draw the following general trend: if homogeneous morphologies may correspond to objects with a high degree of alloying, unevenly shaped samples are characteristic of inhomogeneous composition distributions. Our results show that, as for sample S20, prepared following an *in-situ* seed-mediated approach, anisotropic growth may be promoted at the expense of composition fluctuations which arise at the nanoscale level.

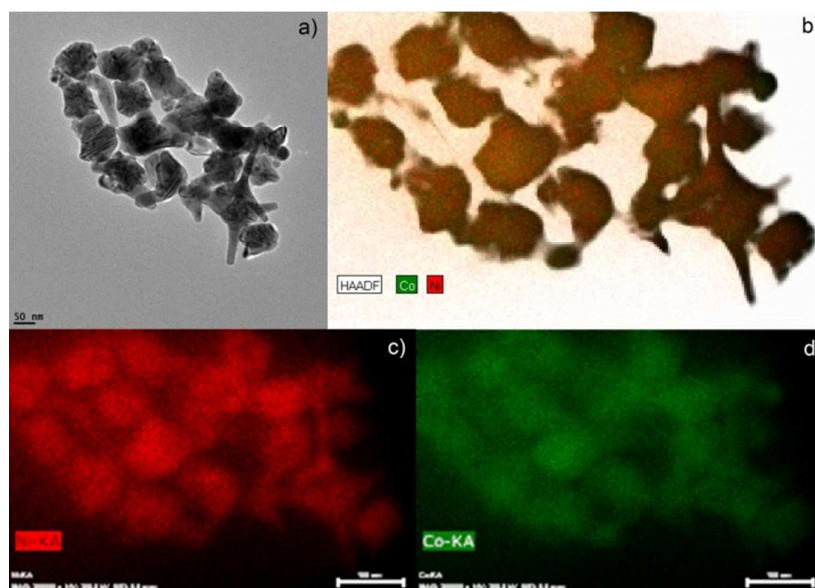


Fig. 6 a) HRTEM image for sample S10, b) HAADF-STEM image. STEM-EDS elemental mapping for Ni, Co [c) and d) respectively].

3.3 Magnetic behaviour

All samples showed room-temperature ferromagnetism and they could easily be magnetically separated from the solvent during the post-preparation stage (Fig. S-14). M-H loops were recorded by SQUID magnetometry at 2 and 300 K for several representative samples. Magnetization values (emu/g) were normalized to metal content, taking into account the elemental analysis results.

Fig. 7 shows M-H loops for samples S17 (isotropic shape) and S6 (anisotropic shape). Sample S17 displays a saturation magnetization M_s equal to ~ 102 emu/g and a coercivity H_c of ~ 150 Oe at room temperature while for sample S6 M_s is equal to ~ 112 emu/g and H_c is equal to 220 Oe. The bulk M_s value for $\text{Ni}_{50}\text{Co}_{50}$ alloy is not available in the literature, however, it can be calculated on the assumption that it linearly depends on the Ni/Co ratio. A value of ~ 111.5 emu/g is thus obtained.¹⁴ We observed that the nearly spherical ~ 65 nm particles of S17 have a somewhat lower M_s than the bulk, while the larger anisotropic structures of S6 yield a M_s value similar to the estimated 'bulk' one. Besides, the smaller isotropic particles of sample S3 ($d < 8$ nm) possess a quite lower saturation magnetization at ~ 70 emu/g (Fig. S-15d in ESI), and a low coercivity (~ 20 Oe) at room temperature. It has been reported that the size of single domain for NiCo system, associated with maximum coercivity and magnetization values, lies in the 30-40 nm range. Particle sizes below or above this range are often related with slightly deteriorated magnetic features.⁶³ However, it is difficult to establish a general trend for the magnetic properties of NiCo nanoparticles of various sizes because the synthetic procedure can also certainly affect the final characteristics of the material. Attempting a comparison with literature, and taking into account the aforementioned restrictions because of the different synthetic conditions, we note that: i) in the case of small NiCo nanoparticles (*i.e.* below the critical grain size,) Sharma *et al.* have reported a zero coercivity at room temperature for stoichiometric ~ 25 nm particles,⁶ while Zhu *et al.* recorded a ~ 100 Oe H_c value for NiCo nanoparticles with a size in the 3-25 nm range.⁶³ The observed H_c value of ~ 20 Oe for sample S3 (size $\sim 2-7$ nm) lies between the above literature values. Concerning the effect of shape anisotropy of sample S6 and its relation to an increased coercivity, one can refer to the work of Thongmee *et al.*, where NiCo nanowires prepared by electrodeposition reached a coercivity of 512 Oe.⁶⁴ In our case, the low room-temperature coercivity of sample S3 can be attributed to its

small particle size, while the relatively high coercivity of sample S6 is consistent with its shape anisotropy.

Fig. S-15 in ESI presents the respective hysteresis loops also for the samples S15, S18 and S19. These samples possess M_s values near 110 emu/g at room temperature, which are slightly increased at 2 K. It seems that the reaction conditions used in these cases do not provide a 'deleterious' environment for the magnetic properties of NiCo nanostructures. Yet, in previously published studies, some ligands such as TOPO have been reported to reduce the surface magnetism.⁶⁵ Furthermore, the SQUID samples are measured in Ar-sealed gelatin capsules, thus hindering the formation of surface oxides, that could also affect the magnetic properties. Samples S15 and S19 present similar coercivity values (~ 180 Oe at room temperature), due to their similar anisotropic morphology. The slightly increased room-temperature value of H_c for sample S18 (~ 220 Oe) can be attributed to the observed tendency for a partial formation of nanowires in this sample, which induced a higher shape anisotropy factor. Targeting to a more extended comparison with literature, a coercivity value of ~ 210 Oe at room temperature was recently recorded for three-dimensional stoichiometric NiCo nanoflowers prepared by a hydrothermal approach.⁶⁶ In our case, coercivity values are certainly also increased at 2 K for all samples, for instance the S18 nanostructures reach a H_c value of ~ 240 Oe at this temperature.

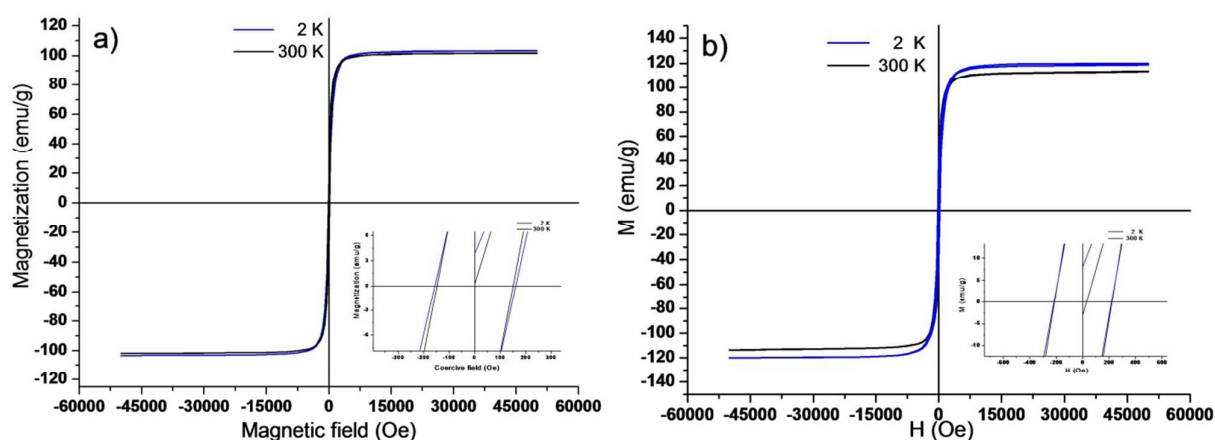


Fig. 7 Hysteresis loops for samples S17 (a) and S6 (b) recorded by SQUID magnetometer

4 Conclusions

This work reports a number of metal-organic chemical routes for the synthesis of NiCo alloy nanostructures. This was a challenging goal, taking into account that apart from the control of the alloy composition, the tailoring of the shape *via* anisotropic growth should also be achieved. The choice of suitable synthesis conditions is fundamental for the above objective. We managed to obtain several anisotropic nanostructures, for instance either by employing homologous precursor pairs and proper acid/amine surfactants, or by heating non-homologous precursors in pure oleylamine. A high degree of homogeneous alloying is evidenced in many cases, although a uniform composition distribution may not be always readily acquired, even after using homologous precursor pairs. Moreover, we have shown that apart from ‘macroscopic’ characterization methods such as ICP elemental analysis and XRD, HRTEM-EDS was also necessary for an accurate composition characterization of the structures at the nanoscale. The *in-situ* seed-mediated approach seems promising for the tailored growth of high-aspect-ratio NiCo nanostructures, nevertheless additional research effort is needed so as to simultaneously improve the alloy composition homogeneity. The NiCo nanostructures of this work present ferromagnetic characteristics, with high saturation magnetization values, close to the ‘bulk’ in most of the cases. Elongated nanostructures exhibit high coercivity values due to their shape anisotropy. Applications in catalysis can be envisaged, especially for the anisotropic nanoalloys or for the smaller spherical particles possessing high surface area.

Acknowledgements

The authors are grateful to the “Service Commun de Microscopie Electronique de L’Université Paul Sabatier” (TEMSCAN). L. Vendier and A. Mari are acknowledged for XRD and SQuID measurements respectively. We thank P. Lecante (CEMES, Toulouse) for the WAXS spectra. This research was supported by the Centre National de la Recherche Scientifique, CNRS. This work was achieved in the frame of French research program PREFACE (PROjet d’Etude Foudre sur Avion Composite plus Electrique). The authors also thank financing French Ministries of Defense (DGA) and Industry (DGCIS), as well as the sponsors which are ASTECH: Hispano-Suiza, AESE: Safran Engineering Service, PEGASE: Eurocopter, and all partners involved in the project.

Electronic Supplementary Information (ESI)

Supplementary data associated with this article, such as TEM images, WAXS patterns, EDS measurements and SQuID loops are available in the online version at:

References and Notes

- 1 D. Wang and Y. Li, *Adv. Mater.*, 2011, **23**, 1044.
- 2 T. Krenke, E. Duman, M. Acet, E.F. Wasserman, X. Moya, L. Manosa and A. Planes, *Nat. Mater.*, 2005, **4**, 450.
- 3 D. Xu, Z. Liu, H. Yang, Q. Liu, J. Zhang, J. Fang, S. Zou and K. Sun, *Angew. Chem. Int. Ed.*, 2009, **48**, 4217.
- 4 R. Ferrando, J. Jellinek and R.L. Johnston, *Chem. Rev.*, 2008, **108**, 845.
- 5 B. Lim, H. Kobayashi, T. Yu, J. Wang, M.J. Kim, Z.-Y. Li, M. Rycenga and Y. Xia, *J. Am. Chem. Soc.*, 2010, **132**, 2506.
- 6 S. Sharma, N.S. Gajbhiye and R.S. Ningthoujam, *J. Colloid Interf. Sci.*, 2010, **351**, 323.
- 7 D. Ung, G. Viau, C. Ricolleau, F. Warmont, P. Gredin and F. Fievet, *Adv. Mater.*, 2005, **17**, 338.
- 8 M.J. Hu, B. Lin and S.H. Yu, *Nano Res.*, 2008, **1**, 303.
- 9 A. Atkinson, S. Barnett, R.J. Gorte, J.T.S. Irvine, A.J. McEvoy, M. Mogensen, S.C. Singhal and J. Vohs, *Nat. Mater.*, 2004, **3**, 17.
- 10 L. Zhang, J.A. Bain, J.-G. Zhu, L. Abelman, and T. Onoue, *J. Appl. Phys.*, 2006, **100**, 053901.
- 11 T. Onoue, M.H. Siekman, L. Abelman, and J.C. Lodder, *J. Magn. Magn. Mater.*, 2005, **287**, 501.
- 12 Q. Liu, X. Guo, T. Wang, Y. Lin and W. Shen, *Mater. Lett.*, 2010, **64**, 1271.
- 13 G. Viau, F. Ravel, O. Acher, F. Fievet-Vincent and F. Fievet, *J. Appl. Phys.*, 1994, **76**, 6570.
- 14 P. Toneguzzo, G. Viau, O. Acher, F. Guillet, E. Bruneton, F. Fievet-Vincent and F. Fievet, *J. Mater. Sci.*, 2000, **35**, 3767.
- 15 P. Saravanan, T.A. Jose, P.J. Thomas and G.U. Kulkarni, *B. Mater. Sci.*, 2001, **24**, 515.
- 16 C. Luna, M.P. Morales, C.J. Serna and M. Vazquez, *Nanotechnology*, 2003, **14**, 268.
- 17 D. Ung, G. Viau, F. Fievet-Vincent, F. Herbst, V. Richard and F. Fievet, *Prog. Solid State Ch.*, 2005, **33**, 137.
- 18 O.D. Jayakumar, H.G. Salunke and A.K. Tyagi, *Solid State Commun.*, 2009, **149**, 1769.
- 19 N. Chakroune, G. Viau, C. Ricolleau, F. Fievet-Vincent and F. Fievet, *J. Mater. Chem.*, 2003, **13**, 312.
- 20 G. Viau, F. Fievet-Vincent and F. Fievet, *Solid State Ionics*, 1996, **84**, 259.
- 21 S. Panday, B.S.S. Daniel and P. Jeevanandam, *J. Magn. Magn. Mater.*, 2011, **323**, 2271.
- 22 P. Elumalai, H.N. Vasan, M. Verelst, P. Lecante, V. Carles and P. Tailhades, *Mater. Res. Bull.*, 2002, **37**, 353.
- 23 Y. Soumare, J.Y. Piquemal, T. Maurer, F. Ott, G. Chaboussant, A. Falqui and G. Viau, *J. Mater. Chem.*, 2008, **18**, 5696.

- 24 D.-E. Zhang, X.-M. Ni, X.-J. Zhang and H.-G. Zheng, *J. Magn. Magn. Mater.*, 2006, **302**, 290.
- 25 S. Pan, Z. An, J. Zhang and G. Song, *Mater. Chem. Phys.*, 2010, **124**, 342.
- 26 M. Wen, Y.-F. Wang, F. Zhang and Q.-S. Wu, *J. Phys. Chem. C.*, 2009, **113**, 5960.
- 27 M. Cheng, M. Wen, S. Zhou, Q. Wu and B. Sun, *Inorg. Chem.*, 2012, **51**, 1495.
- 28 T. Yamauchi, Y. Tsukuhara, K. Yamada, T. Sakata and Y. Wada, *Chem. Mater.*, 2011, **23**, 75.
- 29 S. Zhou, M. Wen, N. Wang, Q. Wu and L. Cheng, *J. Mater. Chem.*, 2012, **22**, 16858.
- 30 F. Dumestre, B. Chaudret, C. Amiens, M.-C. Fromen, M.-J. Casanove, P. Renaud and P. Zurcher, *Angew. Chem. Int. Ed.*, 2002, **41**, 4286.
- 31 N. Cordente, C. Amiens, B. Chaudret, M. Respaud, F. Senocq and M.-J. Casanove, *J. Appl. Phys.*, 2003, **94**, 6358.
- 32 C. Barriere, K. Piettre, V. Latour, O. Margeat, C.-O. Turrin, B. Chaudret and P. Fau, *J. Mater. Chem.*, 2012, **22**, 2279.
- 33 V. Latour, A. Maisonnat, Y. Coppel, V. Colliere, P. Fau and B. Chaudret, *Chem. Commun.*, 2010, **46**, 2683.
- 34 O. Margeat, D. Ciuculescu, P. Lecante, M. Respaud, C. Amiens and B. Chaudret, *Small*, 2007, **3**, 451.
- 35 M. Cokoja, H. Parala, A. Birkner, R.A. Fischer, O. Margeat, D. Ciuculescu, C. Amiens, B. Chaudret, A. Falqui and P. Lecante, *Eur. J. Inorg. Chem.*, 2010, **2010-11**, 1599.
- 36 C. Desvaux, P. Lecante, M. Respaud and B. Chaudret, *J. Mater. Chem.*, 2010, **20**, 103.
- 37 A.V. Trunova, J. Lindner, R. Meckenstock, M. Spasova, M. Farle, D. Ciuculescu, C. Amiens, B. Chaudret and M. Respaud, *J. Magn. Magn. Mater.*, 2009, **321**, 3502.
- 38 S. Mourdikoudis, K. Simeonidis, K. Gloystein, M. Angelakeris, C. Dendrinou-Samara, I. Tsiaoussis and O. Kalogirou, *J. Magn. Magn. Mater.*, 2009, **321**, 2723.
- 39 S. Mourdikoudis, A. Shavel, B. Rodriguez-Gonzalez, C. Serra, K. Simeonidis, M. Angelakeris, C. Dendrinou-Samara and O. Kalogirou, *Polyhedron*, 2009, **28**, 3284.
- 40 S. Mourdikoudis, V. Colliere, C. Amiens, P. Fau and M.L. Kahn, *Langmuir*, 2013, **29**, 13491.
- 41 D. Ung, Y. Soumare, N. Chakroune, G. Viau, M.-J. Vaulay, V. Richard and F. Fievet, *Chem. Mater.*, 2007, **19**, 2084.
- 42 C. Wang, S. Peng, L.-M. Lacroix and S. Sun, *Nano Res.*, 2009, **2**, 380.
- 43 (a) D. Ciuculescu, F. Dumestre, M. Comesana-Hermo, B. Chaudret, M. Spasova, M. Farle and C. Amiens, *Chem. Mater.*, 2009, **21**, 3987; (b) D. de Caro, J. S. Bradley, *Langmuir*, 1997, **13**, 3067.
- 44 For example, data concerning the TGA behavior for some of the Co- and Ni- precursors used can be found at: (a) J. D. Desai, S.K Min, K.D. Jung and O.S. Joo, *Appl. Surf. Sci.*, 2006, **253**, 1781; (b) W.T. Cheng and H.W. Cheng, *AIChE J.*, 2009, **55**, 1383; (c) S. Yoon and A. Manthiram, *Electrochem. Solid. St.*, 2009, **12**, A190; (d) A. Nuha, A. Agus, R.A. Razak and T.S. Lee, Synthesis and Characterization of Metal Stearates as Thermo Pro-Oxidative Additives, *Proceedings of the UMT 11th International Annual Symposium on Sustainability Science and Management*, July 2012, Terengganu, Malaysia.

- 45 D. Xu, Z. Liu, J. Liang and Y. Qian, *J. Phys. Chem. B.*, 2005, **109**, 14344.
- 46 L.-M. Lacroix, S. Lachaize, A. Falqui, M. Respaud and B. Chaudret, *J. Am. Chem. Soc.*, 2009, **131**, 549.
- 47 X. Teng, X. Liang, S. Maksimuk and H. Yang, *Small*, 2006, **2**, 249.
- 48 S. Mourdikoudis and L.-M. Liz-Marzan, *Chem. Mater.*, 2013, **25**, 1465.
- 49 H.-H. Lin and K.-M. Chi, *J. Nanosci. Nanotechnol.*, 2011, **11**, 1193.
- 50 N. Poudyal, G.S. Chaubey, C.-B. Rong and J.P. Liu, *J. Appl. Phys.*, 2009, **105**, 07A749 (1-3).
- 51 S. Sun, H. Zeng, D.B. Robinson, S. Raoux, P.M. Rice, S.X. Wang and G. Li, *J. Am. Chem. Soc.*, 2004, **126**, 273.
- 52 F. Wang, A. Dong, J. Sun, R. Tang, H. Yu and W.E. Buhro, *Inorg. Chem.*, 2006, **45**, 7511.
- 53 N. Petchsang, L. Shapoval, F. Vietmeyer, Y. Yu, J.H. Hodak, I.-M. Tang, T.H. Kosel and M. Kuno, *Nanoscale*, 2011, **3**, 3145.
- 54 (a) W. Shi, H. Zeng, Y. Sahoo, T.Y. Ohulchanskyy, Y. Ding, Z.L. Wang, M. Swihart and P.N. Prasad, *Nano Lett.*, 2006, **6**, 875; (b) W. Baaziz, B.P. Pichon, S. Fleutot, Y. Liu, C. Lefevre, J.-M. Greneche, M. Toumi, T. Mhiri and S. Begin-Colin, *J. Phys. Chem. C*, 2014, **118**, 3795.
- 55 (a) S.A. Simon, *J. Gen. Physiol.*, 1977, **70**, 123; (b) S. Ghosh, R.K. Sahu and C.R. Raj, *J. Mater. Chem.*, 2011, **21**, 11973.
- 56 Y.-N. Wang, W.-T. Wei, C.-W. Yang and M. H. Huang, *Langmuir*, 2013, **29**, 10491.
- 57 K. P. Rice, A. E. Saunders and M. P. Stoykovich, *J. Am. Chem. Soc.*, 2013, **135**, 6669.
- 58 J. Xiao and L. Qi, *Nanoscale*, 2011, **3**, 1383.
- 59 L.-P. Zhu, H.-M. Xiao and S.-Y. Fu, *Eur. J. Inorg. Chem.*, **2007**, 3947.
- 60 N.A.M. Barakat, K.A. Khalil, I.H. Mahmoud, M.A. Kanjwal, F.A. Sheikh and H.Y. Kim, *J. Phys. Chem. C*, 2010, **114**, 15589.
- 61 H. Zhang, T. Yao, Z. Sun, Y. Li, Q. Liu, F. Hu, Z. Pan, B. He, Z. Xie and S. Wei, *J. Phys. Chem. C.*, 2010, **114**, 13596.
- 62 M. Hansen, in *Constitution of Binary Alloys*; McGraw-Hill Book Company, Inc, New York, 1958, pp. 674–677.
- 63 S. Zhu, K. Sun, Q.Y. Zhang, X.T. Zu, L.M. Wang and R.C. Ewing, *J. Appl. Phys.*, 2003, **94**, 5648.
- 64 S. Thongmee, H.L. Pang, J.B. Yi, J. Ding, J.Y. Lin and L.H. Van, *Acta Mater.*, 2009, **57**, 2482.
- 65 N. Cordente, M. Respaud, F. Senocq, M.-J. Casanove, C. Amiens and B. Chaudret, *Nano Lett.*, 2001, **1**, 565.
- 66 M.Y. Rafique, L. Pan, W.S. Khan, M.Z. Iqbal, H. Qiu, M.H. Farooq, M. Ellahi and Z. Guo, *CrystEngComm*, 2013, **13**, 5314.

Table 1: Summary of the reaction parameters for all NiCo samples prepared in this study*

Sample/Fig.	Precursors	Surfactants (eq. ratio)	Solvent	T (°C)	Time	Morphology/size
S1/S-1a	Ni(COD) ₂ , Co(COD)(COT)	HDA (10 eq)	Anisole	150	24 h	Large aggregates
S2/S-1b	Ni(COD) ₂ , {Co[N(SiMe ₃) ₂] ₂ } ₂	HDA (10 eq)	Anisole	150	24 h	Large aggregates
S3/1	Ni(COD) ₂ , Co(COD)(COT)	ACA/HDA (1/2) / 1 metal	Anisole	150	24 h	Bimodal size 7.1 ± 1.1, 2.5 ± 0.5 nm
S4/S-2	Ni(COD) ₂ , {Co[N(SiMe ₃) ₂] ₂ } ₂	ACA/HDA (1/2) / 1 metal	Anisole	150	24 h	Bimodal size 6.1 ± 1.4, 2.4 ± 0.7 nm
S5/S-3	Ni(COD) ₂ , Co(COD)(COT)		EDA	120	48 h	Polydisperse 12.2 ± 5.8 nm NPs and aggregates
S6/S-4	Ni-acetate, Co-acetate	ACA/HDA (1/2) / 1 metal	Anisole	150	24 h	Elongated shapes <i>l</i> ~ 250-300, <i>d</i> ~ 60-90 nm
S7/S-5	Ni-acetate, Co-acetate	ACA/HDA (2/1) / 1 metal	Anisole	150	24 h	Nanospatulas, <i>l</i> ~ 650-850, <i>d</i> ~ 70-160 nm
S8/2a	Ni(COD) ₂ , Co(COD)(COT)		OAm	240	45 min	Bimodal isotropic/ 7.2±1.3 & 2.4±0.5 nm
S9/2b	Ni-acetate, Co-acetate		OAm	240	45 min	Multiangular 120±25 nm
S10/S-6b	Ni(acac) ₂ , Co(acac) ₃		OAm	240	45 min	Multiangular 93±13 nm
S11/S-6a	Ni-stearate, Co-stearate		OAm	240	45 min	Multiangular 67±12 nm
S12/S-7a	Ni-stearate, Co-stearate		TOAm	240	45 min	Mainly large aggregates
S13/S-7b	Ni(acac) ₂ , Co(acac) ₃		TOAm	240	45 min	Mainly large aggregates
S14/4b	Ni(acac) ₂ , Co(acac) ₃	OAc (1 eq.)	OAm	240	45 min	Nanospheres 2.4 ± 1 nm
S15/S-8	Ni-stearate, Co-stearate	ACA (2 eq.)	OAm	240	45 min	Multiangular 83 ± 16 nm
S16/3b	Ni-acetate, Co-acetate	ACA/HDA (1/2) / 1 metal	hexadecane	240	45 min	Long nanowires and some particles
S17/S-9	Ni-stearate, Co-stearate	HDA (2 eq to total metal eq)	hexadecane	240	45 min	'smooth-angled' 65 ± 11 nm NPs & aggregates
S18/S-10	Ni(acac) ₂ , Co(acac) ₃	HDA (2 eq.)	Octyl ether	240	45 min	Mainly multiangular 76±13 nm
S19/3a	Ni(acac) ₂ , Co-stearate		OAm	240	45 min	Multiangular 52±2.5 nm
S20/4a	Ni(COD) ₂ , Co-stearate		OAm	240	45 min	NWs (<i>l</i> ~300-600 nm), NRs (<i>l</i> <300, <i>d</i> ~ 10 nm)

*H₂ was used as reducing agent in all samples. NPs = nanoparticles, OAc=oleic acid, OAm=oleylamine, TOAm=trioctylamine, EDA=ethylenediamine, HDA=hexadecylamine, ACA=1-adamantanecarboxylic acid.